ARTICLE

Development of a Model Protein Interaction Pair as a Benchmarking Tool for the Quantitative Analysis of 2-Site Protein-Protein Interactions

Aaron P. Yamniuk,[1] John A. Newitt,[1] Michael L. Doyle,[1] Fumio Arisaka,[2] Anthony M. Giannetti,[3] Preston Hensley,[4] David G. Myszka,[5] Fred P. Schwarz,[6] James A. Thomson,[7] and Edward Eisenstein[8]

[1]Bristol-Myers Squibb, Princeton, New Jersey 08540, USA; [2]Tokyo Institute of Technology, Yokohama 226-8503, Japan; [3]Google[x], Google Life Sciences, Mountain View, California 94043, USA; [4]SystaMedic, Incorporated, Groton, Connecticut 06340, USA; [5]Biosensor Tools LLC, Salt Lake City, Utah 84103, USA; [6]National Institute of Standards and Technology, Gaithersburg, Maryland 20899, USA; [7]Polaris Pharmaceuticals, Incorporated, San Diego, California 92121, USA; and [8]Institute for Bioscience and Biotechnology Research, Fischell Department of Bioengineering, University of Maryland, Rockville, Maryland 20850, USA

A significant challenge in the molecular interaction field is to accurately determine the stoichiometry and stepwise binding affinity constants for macromolecules having >1 binding site. The mission of the Molecular Interactions Research Group (MIRG) of the Association of Biomolecular Resource Facilities (ABRF) is to show how biophysical technologies are used to quantitatively characterize molecular interactions, and to educate the ABRF members and scientific community on the utility and limitations of core technologies [such as biosensor, microcalorimetry, or analytic ultracentrifugation (AUC)]. In the present work, the MIRG has developed a robust model protein interaction pair consisting of a bivalent variant of the *Bacillus amyloliquefaciens* extracellular RNase barnase and a variant of its natural monovalent intracellular inhibitor protein barstar. It is demonstrated that this system can serve as a benchmarking tool for the quantitative analysis of 2-site protein-protein interactions. The protein interaction pair enables determination of precise binding constants for the barstar protein binding to 2 distinct sites on the bivalent barnase binding partner (termed binase), where the 2 binding sites were engineered to possess affinities that differed by 2 orders of magnitude. Multiple MIRG laboratories characterized the interaction using isothermal titration calorimetry (ITC), AUC, and surface plasmon resonance (SPR) methods to evaluate the feasibility of the system as a benchmarking model. Although general agreement was seen for the binding constants measured using solution-based ITC and AUC approaches, weaker affinity was seen for surface-based method SPR, with protein immobilization likely affecting affinity. An analysis of the results from multiple MIRG laboratories suggests that the bivalent barnase-barstar system is a suitable model for benchmarking new approaches for the quantitative characterization of complex biomolecular interactions.

Key Words: analytical ultracentrifugation, isothermal titration calorimetry, surface plasmon resonance

INTRODUCTION

Knowledge of protein-protein binding affinities is important in elucidating biologic processes in living cells, relating protein structure to function, and in rational protein drug design. Some of the common methods to measure the affinity of biomolecular interactions include isothermal titration calorimetry (ITC), analytic ultracentrifugation (AUC), and optical biosensors such as those based on the principles of surface plasmon resonance (SPR). Although quantitative determination of the K_d for biomolecular interactions using these methods is commonplace, there is a need to not only evaluate but also to validate these methods, as well as other quantitative approaches, by a comparison of interaction data obtained using multiple orthogonal methods. In particular, it is important for users to be aware of the limitations of each technology and how these limitations relate to user experience, instrument performance (maintenance and calibration), solution, and experimental conditions, as well as the specific experimental system of interacting molecules. The expertise required for the evaluation and validation of these methods is often found in core facilities. Accordingly, the Association of Biomolecular Resource Facilities (ABRF) established the Molecular Interactions Research Group (MIRG; see ABRF Web site at www.abrf.org and MIRG Web site at www.abrf.org/MIRG) to further develop methodologies to measure quantitatively

Address correspondence to: Aaron Yamniuk, Bristol-Myers Squibb, Route 206 and Provinceline Road, Princeton, NJ 08540, USA (Phone: 609-252-5342; Fax: 609-252-6012; E-mail: aaron.yamniuk@bms.com).
doi: 10.7171/jbt.15-2604-001

ligand-protein and protein-protein interactions, and to educate the community on the utilization of these technologies and their limitations.

In an earlier benchmarking study, the MIRG evaluated the capabilities of different participant laboratories to apply the core molecular interaction technologies of ITC and SPR to quantitatively characterize the binding of the small molecule inhibitor 4-carboxybenzenesulfonamide (CBS) to bovine carbonic anhydrase II (CA-II), as well as to use AUC to characterize the oligomeric state of CA-II.[1] This protein-ligand pair was selected because it represented a simple and well-characterized 1:1 binding interaction, and the reactants were readily available and well behaved with high solubility and stability. The results of the study showed that when the experiments were carefully performed and the data correctly interpreted, the true binding affinity could be accurately obtained using each technology. More recently, the MIRG developed a ternary protein-protein interaction system that enabled users of biomolecular interaction technologies to evaluate whether 2 proteins that bind to a third protein bind competitively or form a ternary complex.[2]

A critically important aspect of developing protein interaction systems is that the proteins need to be easy and inexpensive to produce with high yield, as well as highly stable and soluble. In the present work, we have the additional challenge of developing a protein interaction pair in which 1 binding partner contains 2 binding sites having very different binding affinities, both of which also need to be in an affinity range that is accessible by common biophysical technologies.

The protein-protein interaction system evaluated by the MIRG for this purpose utilizes variants of the *Bacillus amyloliquefaciens* extracellular RNase barnase and its natural intracellular inhibitor protein barstar. Both proteins are small (10–12 kDa) and monomeric in solution, with high stability and solubility. The interaction between the wild-type proteins has been extensively characterized by structural and biophysical methods and shown to be among the highest affinity interactions known for a protein-protein pair, with a K_d of $\sim 10^{-14}$ M.[3] In addition, dozens of single amino acid mutations and combinations of mutations have been identified in each protein that can modify the binding affinity over a broad range spanning from the wild-type at 10^{-14} M to as low as 10^{-4} M for weakly associating variants.[4–8] Moreover, it has been shown that 2 mutant barnase proteins can be fused with a short linker to produce bivalent barnase proteins termed "binases," with each domain capable of binding to a separate barstar protein.[2,9]

In the present study, the MIRG selected a mutant barstar-binase interaction pair that could be used to evaluate molecular interaction technologies over an affinity range typical of the interactions studied in most core facilities: K_d $\sim 10^{-9}$–10^{-5} M. Here, a "higher-affinity" barnase domain containing a single H102Q mutation and a "lower-affinity" barnase double-mutant containing R59A and H102Q mutations were fused together in each of 2 orientations to generate binase1 (R59A,H102Q—H102Q) and binase2 (H102Q—R59A,H102Q) (**Fig. 1**). For barstar, the double-cysteine mutation [C40A, C82A—hereafter indicated with an asterisk (*)] was incorporated to facilitate efficient cysteine-free protein production,[10,11] along with a Y29A mutation that has been shown to reduce the barnase binding affinity by ~1 order of magnitude compared with the wild-type protein.[4,8] The binding of the resulting triple mutant (barstar*-Y29A) to binase1 and binase2 was then characterized using the 3 core label-free interaction technologies of ITC, AUC, and SPR. For comparison, the cysteine-free protein having wild-type binding activity (barstar*) was also generated and tested. The results of these studies are presented, and

his-barstar*

*M*GSHHHHHDSENLYFQG KKAVINGEQI RSISDLHQTL KKELALPEYY GENLDALWDA
LTGWVEYPLV LEWRQFEQSK QLTENGAESV LQVFREAKAE
GADITIILS

his-barstar*-Y29A

*M*GSHHHHHDSENLYFQG KKAVINGEQI RSISDLHQTL KKELALPEAY GENLDALWDA
LTGWVEYPLV LEWRQFEQSK QLTENGAESV LQVFREAKAE
GADITIILS

his-binase1

*M*GSHHHHHHSENLYFQG AQVINTFDGV ADYLQTYHKL PDNYITKSEA QALGWVASKG
NLADVAPGKS IGGDIFSNAE GKLPGKSGRT WREADINYTS
GFRNSDRILY SSDWLIYKTT DQYQTFTKIR GSNTFDGVAD
YLQTYHKLPD NYITKSEAQA LGWVASKGNL ADVAPGKSIG
GDIFSNREGK LPGKSGRTWR EADINYTSGF RNSDRILYSS
DWLIYKTTDQ YQTFTKIR

his-binase2

*M*GSHHHHHHSENLYFQG AQVINTFDGV ADYLQTYHKL PDNYITKSEA QALGWVASKG
NLADVAPGKS IGGDIFSNRE GKLPGKSGRT WREADINYTS
GFRNSDRILY SSDWLIYKTT DQYQTFTKIR GSNTFDGVAD
YLQTYHKLPD NYITKSEAQA LGWVASKGNL ADVAPGKSIG
GDIFSNAEGK LPGKSGRTWR EADINYTSGF RNSDRILYSS
DWLIYKTTDQ YQTFTKIR

FIGURE 1

Barstar and binase amino acid sequences. Color coding is as follows: N-terminal TEV-cleavable poly-His tag is in red, additional nonnative residues remaining after TEV cleavage are in black, barstar domains are in blue, mutant barnase domains are in green, and GS linker connecting mutant barnase domains in the binase proteins is in orange. Mutations from the wild-type barstar and barnase sequences are underlined, including barstar mutations Y29A, C40A, C82A, and barnase mutations R59A and H102Q. Both barstar constructs also contain an H→D mutation in the His tag (underlined), which was unintentionally introduced during cloning. The N-terminal methionine (italicized) is processed during expression and is not present in the final products.

the suitability of the barstar*-Y29A-binase protein interaction pair for future use in benchmarking of users' ability to quantitatively characterize complex biomolecular interactions is discussed.

MATERIALS AND METHODS

Proteins

The protein material used for the studies was produced and characterized in different laboratories over the course of several years. Batch A material was studied by laboratories A and B, whereas batch B material was generated several years earlier and characterized in laboratories C, D, E, F, and G. The protocols used for expression and purification of the barstar and binase proteins were adapted from those reported previously.[2,12] A detailed protocol is given below for purification of batch A material, with batch B material being produced in a similar manner.

For generation of batch A barstar* and binase proteins, recombinant DNA expression vectors encoding the His-tagged barstar* and His-tagged binase proteins in pET22b (Novagen, EMD Millipore, Billerica, MA, USA) were transformed into competent BL21-Gold(DE3) (Stratagene, La Jolla, CA, USA) and maintained as frozen glycerol stocks. Freshly streaked Luria-Bertani-agar plates with 100 μg/ml carbenicillin were prepared, and single colonies were selected and inoculated into 50 ml starter cultures containing Terrific Broth (TB) medium (Cell-Gro, Mediatech, Incorporated, Corning, Manassas, VA, USA) with 50 μg/ml carbenicillin. After culturing at 37°C in a rotary shaker overnight, the cells from saturated starter cultures were pelleted by sedimentation, resuspended in fresh TB/carbenicillin medium, and a portion of each sample was used to inoculate a 1 L culture of TB/carbenicillin in 2.5 L HiYield shaker flasks (Thomson Instrument Company, Oceanside, CA, USA). The cultures were grown at 37°C and 250 rpm in a rotary shaker (New Brunswick Innova, Eppendorf, New Delhi, India) until an optical density (O.D.) at 600 nm of ~2.5 was achieved. The cultures were then rapidly cooled by placing the flask on ice for 30 minutes, isopropyl β-D-1-thiogalactopyranoside (0.5 mM) was added to each flask, and the cultures were incubated at 18°C with shaking at 230 rpm for 22 hours. The cells (O.D. at 600 nm of ~13.5) were harvested by sedimentation at 6700 × *g* (maximum) for 30 minutes at 4°C. The pellets were frozen and stored at −80°C. Pellet weights from 1 L culture for each construct were ~20 g. SDS-PAGE analysis of aliquots from the harvested cultures confirmed that overexpression of each protein was >100 mg/L.

All purification steps were performed at 4°C unless stated otherwise. For all constructs, the cell pellets were lysed, His-tagged proteins captured by Ni^{2+}-affinity chromatography, and eluted in an identical fashion. Typically, a frozen 20 g pellet was thawed and suspended by rapid stirring in 250 ml of 50 mM 4-(2-hydroxyethyl)-1-piperazineethanesulfonic acid (HEPES), 300 mM NaCl, 5% glycerol, 25 mM imidazole, 2 mM DTT (pH 7.5), and 5 tablets of Complete EDTA-free protease inhibitor cocktail (Roche Diagnostics Corporation, Indianapolis, IN, USA). The chilled suspension was passed through a mechanical homogenizer (APV1000; APV, Delavan, WI, USA) at 800 bar and collected into a vessel on ice. The lysate was clarified by sedimentation at 17,700 × gmax for 1 hour. The clarified lysate was loaded onto a 28 ml column (2.6 × 5.5 cm) of Ni-Sepharose 6 Fast Flow (GE Healthcare Bio-Sciences, Pittsburgh, PA, USA) equilibrated with 50 mM HEPES, 300 mM NaCl, 5% glycerol, and 25 mM imidazole (pH 7.5). The column was washed extensively with the same buffer until the absorption at 280 nm neared the baseline. The His-tagged protein was eluted with 50 mM HEPES, 300 mM NaCl, 5% glycerol, and 300 mM imidazole (pH 7.5).

The His-tagged barstar* proteins that eluted from the Ni^{2+}-affinity column were supplemented with 1 mM EDTA, concentrated by ultrafiltration (Amicon Ultra 3 kDa cutoff; EMD Millipore, Billerica, MA, USA), and purified in 3 lots by size exclusion chromatography (SEC) on a HiLoad 26/60 Superdex 75 pep grade column (GE Healthcare Bio-Sciences, Pittsburgh, PA, USA) equilibrated with 50 mM Tris-HCl, 50 mM NaCl, and 0.5 mM EDTA (pH 8.0). Fractions from the monomer peak eluting from the SEC column at 200 ml were pooled from each of the 3 runs. This protein was purified further in 2 lots by anion exchange chromatography on a 17 ml column (1.6 × 8.5 cm) of SOURCE 15Q (GE Healthcare Bio-Sciences) equilibrated with 50 mM Tris-HCl, 50 mM NaCl, and 0.5 mM EDTA (pH 8.0) and eluted with a linear gradient of NaCl to 250 mM. Peak fractions in the gradient between 55 and 135 mM NaCl were pooled from each run. Final purified yields for the His-tagged barstar* proteins were ~400 mg/L *Escherichia coli* culture.

The His-tagged binase proteins from the Ni^{2+}-affinity column were supplemented with 1 mM EDTA, concentrated by ultrafiltration (Amicon Ultra 10 kDa cutoff; EMD Millipore), and exchanged into 20 mM sodium acetate and 250 mM NaCl (pH 5.0) by chromatography on a HiPrep 26/10 Fast Desalting column (GE Healthcare Bio-Sciences). The excluded volume peak containing the His-tagged binase proteins developed a fine precipitate after storage on ice overnight (comprised primarily of contaminating proteins and nonproteinaceous material) that was removed by passing the sample through an

Acrodisc Supor 0.22 μm syringe filter (Pall Corporation, Port Washington, NY, USA). Each protein was diluted with 3.5 volumes of 20 mM sodium acetate, 50 mM NaCl (pH 5.0) to reduce the concentration of NaCl to ~95 mM, and loaded in 2 lots onto a 17 ml cation exchange column (1.6 × 8.5 cm) of SOURCE 15S (GE Healthcare Bio-Sciences) and eluted with a gradient of 50–500 mM NaCl in 20 mM sodium acetate (pH 5.0). Fractions from the peak containing the purified His-tagged binase protein eluted late in the gradient (~295–325 mM NaCl) were pooled. The protein was concentrated and then exchanged back into 50 mM Tris-HCl, 100 mM NaCl, and 0.5 mM EDTA (pH 8.0) by Fast Desalting chromatography. The final yield of purified His-tagged binase proteins was ~85 mg/L *E. coli* culture.

A 5 mg portion of each of the His-tagged proteins was treated with AcTEV (Invitrogen, Waltham, MA, USA) protease (1000 U/mg) for 18 hours at 23°C to remove the His tag. The cleavage reactions were supplemented with 1 mM $MgCl_2$ and were purified by passing through a 1 ml gravity column of Ni^{2+}-Sepharose 6 Fast Flow equilibrated with 50 mM Tris-HCl (pH 8.0) and 100 mM NaCl. The cleaved barstar* proteins were eluted in the flow-through fraction and with a 3-bed volume wash with 50 mM Tris-HCl (pH 8.0) and 100 mM NaCl. The 2 cleaved binase proteins were slightly more retained, and flow-through elutions were pooled with a 3-bed volume elution with 50 mM HEPES, 300 mM NaCl, 5% glycerol, and 25 mM imidazole (pH 7.5).

Production of batch B protein material was similar to batch A except that the barstar* protein was expressed without the N-terminal His tag, in *E. coli* strain HB101 containing the pMT643 plasmid. Here, cells expressing barstar* were lysed by lysozyme treatment followed by 3 freeze-thaw cycles, and the cell lysate supernatant pH was adjusted to ~8–8.5 with NH_4OH. The lysate was then centrifuged for 20 minutes at 15,000 rpm to remove debris and then $(NH_4)_2SO_4$ was added to the supernatant to only 40% saturation. After centrifugation at 15,000 rpm for 20 minutes, additional $(NH_4)_2SO_4$ was added to the supernatant up to 80% saturation. The resulting pellet was resuspended in a minimal volume of 20 mM $NH_4C_2H_3O_2$ at pH 8.0 and dialyzed. The dialysate was centrifuged at 15,000 rpm for 15 minutes to remove pellet particulates and then applied to a Q-Sepharose 75 column (GE Healthcare Bio-Sciences) to elute the barstar* with a linear gradient from 0 to 200 mM NaCl in 20 mM $NH_4C_2H_3O_2$ at pH 8.0.

All of the purified proteins, with and without His tags, were exchanged into the final storage buffer [50 mM ammonium acetate, 100 mM NaCl, 0.1 mM EDTA, and 0.01% sodium azide (pH 8.0)] by desalting chromatography and dialysis. Proteins were confirmed to be >95% pure by SDS-PAGE, and mass identification was confirmed by mass spectrometry, in addition to the other confirmations of purity and oligomeric state that are described in the RESULTS. The proteins prepared and stored in this manner were stable at 4°C for several years.

SEC Coupled to Multiangle Laser Light Scattering

SEC-multiangle laser light-scattering (MALS) experiments were performed using a Shodex Protein KW 803 column (8 × 300 mm; Showa Denko America, Incorporated, New York, NY, USA), connected to an Agilent 1100 series HPLC (Agilent Technologies, Santa Clara, CA, USA) in buffer containing 200 mM K_2HPO_4 and 150 mM NaCl (pH 6.8 with HCl), with 0.02% sodium azide added (0.1 μm filtered) running at 0.5 ml/min. Injections were performed using an Agilent Technologies autosampler, and data were obtained from 3 online detectors connected in series: an Agilent Technologies diode array UV-visible spectrophotometer, followed by a Wyatt Technology Corporation miniDawn 3 angle laser light-scattering detector (Goleta, CA, USA), then a Wyatt Optilab DSP interferometric refractometer (Wyatt Technology Corporation). Data were collected and analyzed using ASTRA (Wyatt Technology Corporation) and ChemStation (Agilent Technologies) software.

Dynamic Light Scattering

Dynamic light-scattering (DLS) studies were performed on a Wyatt DynaPro Plate Reader in 384-well plates at 25°C. Each barstar* and binase protein was analyzed at 1.2 mg/ml in 50 mM ammonium acetate (pH 8.0), 0.1 M NaCl, 0.1 mM EDTA, and 0.01% sodium azide. Experimental parameters were 20 acquisitions of 5 seconds each per measurement, and measurements were recorded in quadruplicate, with the average and SD reported. Intensity autocorrelation functions were fitted using the "Regularization" algorithm in the Dynamics software (Wyatt Technology Corporation).

ITC

ITC experiments were performed using VP-ITC microcalorimetry instrumentation (MicroCal; GE Healthcare Bio-Sciences), in buffer consisting of 50 mM ammonium acetate (pH 8.0), 0.1 M NaCl, 0.1 mM EDTA, and 0.01% sodium azide. Experiments involved sequential injections of concentrated His-tagged or -untagged barstar* or barstar*-Y29A proteins (35–711 μM) into a sample cell containing His-tagged or -untagged binase1

or binase2 at ~20-fold lower concentration (2–35 μM), with constant mixing, at temperatures between 20 and 36°C. Control titrations were performed to determine the heat of dilution of the titrant by titrating identical volumes of the barstar* proteins into buffer, and where necessary, these values were subtracted from the barstar*-binase binding data.[13] Integrated data were fitted using either the "one set of sites" or "two sets of sites" binding model supplied in Origin analysis software (OriginLab, Northampton, MA, USA) to provide values for stoichiometry (N), enthalpy (ΔH), and association constant (K_a) for each of the 2 binding sites, and the K_d values were calculated as $K_d = 1/K_a$.

AUC

Sedimentation equilibrium experiments conducted in laboratory B were performed with a Beckman XL-I analytic ultracentrifuge (Beckman Coulter, Brea, CA, USA) using a 4-hole An60-Ti rotor at 25°C. Data were collected on samples using 2-channel centerpieces at several concentrations and rotor speeds. Concentration distributions for the various proteins were collected at 280 nm after attaining equilibrium, usually between 18 and 24 h at a particular speed, as an average of 25 measurements at each radial position with a nominal spacing of 0.001 cm between radial positions.

The MW of each component was calculated by nonlinear least-squares analysis of the concentration distribution of multiple concentrations at sedimentation equilibrium at several rotor speeds in terms of a single, homogeneous species according to Equation 1:

$$C_r = B + C_m \exp\left[M(1-\nu\rho)\omega^2\left(r^2 - r_m^2\right)/2RT\right] \quad \text{(Equation 1)},$$

where C_r is the concentration of the sample at a particular radial position, C_m is the concentration of the sample at the meniscus, M is the MW, ν is the partial-specific volume of the protein, ρ the solvent density, ω is the angular velocity, r is the radial position in centimeters from the center of rotation, r_m is the distance in centimeters from the center of rotation to the meniscus, R is the gas constant, T is the absolute (Kelvin) temperature, and B is a correction term for a non-zero baseline. The partial-specific volumes of the proteins were calculated from the amino acid compositions, and the solvent density was calculated as 1.00355 g/ml from composition.[14]

The interactions of the barstar and bivalent barnase variants were analyzed at sedimentation equilibrium according to Equation 2:

$$\begin{aligned} C_r = B &+ C_{m,N}\exp\left[M_N(1-\nu_N\rho\ )\omega^2\left(r^2 - r_m^2\right)/2RT\right] \\ &+ C_{m,S}\exp\left[M_S(1-\nu_S\rho)\omega^2\left(r^2 - r_m^2\right)/2RT\right] \\ &+ \left(C_{m,N}C_{m,S}/K_D\right)\exp\left[M_C(1-\nu_C\rho)\omega^2\left(r^2 - r_m^2\right)/2RT\right] \end{aligned} \quad \text{(Equation 2)},$$

where $C_{m,N}$ is the concentration of barnase at the meniscus, M_N is the MW of the barnase variant, ν_N is the partial-specific volume of bivalent barnase, $C_{m,S}$ is the concentration of barstar at the meniscus, M_S is the MW of the barstar variant, ν_S is the partial-specific volume of barstar, M_c is the molecular weight of the complex, ν_c is the partial-specific volume of the complex, and K_D is the equilibrium K_d for the binding of barstar to the second (weaker) affinity site on bivalent barnase. Parameters were evaluated using nonlinear least-squares analysis.[15] Data for 3 different concentrations at 2 rotor speeds were analyzed simultaneously as a test for homogeneity and reversibility[16] and to constrain confidence intervals for the parameter values.[17]

Laboratory B performed both sedimentation velocity and equilibrium experiments using a Beckman Coulter analytic ultracentrifuge. Sedimentation velocity experiments to ensure sample homogeneity were analyzed using Digital Compensator Design Tool (DCDT) from the National Analytical Ultracentrifugation Facility (NAUF) group, DCDT from Philo,[18] SEDANAL from Stafford,[19] SEDFIT from Schuck and Rossmanith,[20] or Lamm developed by Behlke and Ristau.[21] For sedimentation equilibrium, a single c-cell format was used that was equipped with an external-loading 6-channel Yphantis-type centerpiece so that optical blank runs could be performed without dismantling the cells. The samples were monitored at 3 different loading concentrations with equal concentrations of barstar* and binase, using 2 rotor speeds, and analyzed globally. The rotor speeds were 28,000 and 34,000 rpm corresponding to σ values defined by Equation 3, respectively, of 2.8 and 4.0 cm^{-2}:

$$\sigma = \omega^2 S/D = M(1-\nu\rho)\omega^2/RT = d\ln(c)/d\left(r^2/2\right) \quad \text{(Equation 3)},$$

where ω is the angular velocity, S is the sedimentation coefficient, D is the translational diffusion coefficient, M is the molecular mass, υ is the partial-specific volume, ρ is the solvent density, R is the ideal gas constant, T is the temperature in Kelvins, c is the solute concentration, and r is the radial distance from the center of rotation. The sedimentation equilibrium data for the complexes were analyzed in terms of a sum of 2 monomer exponentials and 1 complex exponential for curve fitting of the results to obtain the K_a values for each complex.

SPR

SPR measurements were performed on Biacore 2000, 3000, or T100 optical biosensor instruments at 25°C, using CM5 research-grade sensor chips, and *N*-hydroxysuccinimide (NHS), *N*-ethyl-*N*′-(3-diethylaminopropyl)carbodiimide (EDC), and ethanolamine coupling and blocking reagents (Biacore, GE Healthcare Bio-Sciences). Immobilized binase surfaces were prepared using 5–20 μg/ml binase1 or binase2 in 10 mM sodium acetate (pH 4.5) at various surface densities between 40 and 3000 response units, in a running buffer of 10 mM HEPES and 150 mM NaCl (pH 7.4). Reference surfaces were prepared by activation with EDC-NHS and blocking with ethanolamine.

Kinetic experiments were performed by flowing analyte at concentrations between 0.57 nM and 300 μM over each surface at a flow rate of 50 μl/min, with contact times of 40–60 seconds and dissociation times of 60–180 seconds, in running buffer consisting of 50 mM ammonium acetate (pH 8.0), 0.1 M NaCl, 0.1 mM EDTA, and 0.05% surfactant p20. Barstar*-Y29A dissociated completely from the reaction surfaces during the dissociation time, so there was no need for a regeneration step. However, barstar* dissociation was considerably slower[22] and required surface regeneration between cycles using two 5-second injections of 50 mM NaOH at 30 μl/min. For data in which steady state was achieved during the association phase, data analysis was performed by fitting the data to a 2:1 steady-state binding isotherm using Biacore T100 evaluation software, CLAMP software,[23] or Scrubber2.0 (BioLogic Software, Campbell, Australia) to obtain K_d values for both the low- and high-affinity binding sites. For barstar* experiments in which steady state was not achieved for some of the lower-concentration analyte injections, the analyses of the lower- and higher-affinity binding interactions were analyzed separately to estimate binding affinities. For these experiments, the K_d for the higher-affinity binding site was estimated by fitting the lower-concentration analyte injections (10^{-8}–10^{-10} M) to a 1:1 Langmuir binding model, and the K_d for the lower-affinity binding site was analyzed by fitting the higher-concentration analyte data (10^{-6}–10^{-4} M) to a 1:1 steady-state binding model.

Anti-His capture SPR experiments were performed on a Biacore T100 instrument at 25°C. Surfaces were prepared by immobilizing the Fab fragment from an anti-His_6 antibody (proprietary antibody generated at Bristol-Myers Squibb, Princeton, NJ, USA) at 20 μg/ml in 10 mM sodium acetate (pH 4.5) on flow cells 1 and 2 of a CM5 chip using EDC-NHS coupling with ethanolamine blocking to an immobilization level of ~3500 RU. His-binase2 (5–20 μg/ml) was captured on flow cell 2 using a contact time of 30 s at 10 μl/min, resulting in capture levels of ~300–700 RU. Untagged barstar* or barstar*-Y29A analytes were injected over flow cell 1 (reference surface) and flow cell 2 (active surface) using the same analyte concentrations, association and dissociation times, and flow rates as described above for the amine-coupled binase SPR experiments. Surfaces were regenerated between cycles using 2 pulses of 10 mM glycine (pH 2.0) for 15 seconds at 30 μl/min, and data were analyzed as above for the immobilized binase experiments.

RESULTS

Identity and Oligomeric State of Barstar and Binase Proteins

Barstar and binase proteins were produced in 2 batches, "A" and "B," and were generated either with or without an N-terminal tobacco etch virus (TEV)-cleavable His tag as described in MATERIALS AND METHODS. The amino acid sequences of each protein are shown in Fig. 1, and the predicted mass, molecular volume, extinction coefficient, and isoelectric points (pIs) as calculated based on amino acid sequence are summarized in **Table 1**. The identity of each protein was confirmed by mass spectrometry, and SEC-MALS data confirmed that the proteins were each monomeric in solution. The hydrodynamic radius (Rh) as measured by DLS was also consistent with each protein existing in solution as a monomer, and the Rh for the His-tagged proteins was ~15% larger than for the untagged proteins, consistent with the His tag adopting a flexible extended structure in solution (Table 1). Collectively, these data demonstrate that the barstar and binase protein samples were all of suitable quality for biophysical studies.

ITC Characterization of Barstar*-Binase Interactions

The interaction between barstar and binase proteins in solution was studied by ITC in 3 laboratories: A, C, and D. Representative ITC data for titration of His-barstar*-Y29A into His-binase2 at 25°C are shown in **Fig. 2*A***. Here, it can be seen that early in the titration, the injection of His-barstar*-Y29A generates strong exothermic signals because the protein binds predominantly to the high-affinity site on His-binase2 (the H102Q domain). These signals saturate sharply near a 1:1 stoichiometry as the high-affinity site becomes filled. The subsequent injections generate smaller exothermic signals and a more gradually saturating curve as His-barstar*-Y29A binds to the lower-affinity site on His-binase2 (the R59A,H102Q domain). Simultaneously fitting the data for binding to both sites using a two sets of sites model yields K_d values of 8 nM for the high-affinity site and 3 μM for the low-affinity site (**Table 2**).

TABLE 1

Theoretical and Experimental Properties of Barstar and Binase Proteins

Protein	Batch	Predicted mass (g/M)[a]	Molecular volume (cm^3)	Extinction coefficient ($M^{-1}cm^{-1}$)	Theoretical pI	ESI/TOF mass (g/M)	DLS Rh (nm)	SEC-MALS (g/M)	AUC mass
His-Barstar*	A	12,031	0.7351	2.246×10^4	5.31	12,030	1.8 ± 0.0	12,290	13,807
His-Barstar*-Y29A	A	11,939	0.7355	2.097×10^4	5.31	11,939	1.9 ± 0.1	11,760	13,673
His-Binase1	A	26,283	0.7243	5.535×10^4	8.51	26,284	2.6 ± 0.1	26,690	26,492
His-Binase2	A	26,283	0.7243	5.535×10^4	8.51	26,284	2.6 ± 0.1	27,330	26,534
Barstar*	A	10,205	0.7444	2.097×10^4	4.88	10,205	1.6 ± 0.1	10,060	
Barstar*-Y29A	A	10,112	0.7450	1.948×10^4	4.88	10,112	1.6 ± 0.1	9793	
Binase1	A	24,434	0.7271	5.386×10^4	8.82	24,434	2.2 ± 0.2	24,900	
Binase2	A	24,434	0.7271	5.386×10^4	8.82	24,434	2.3 ± 0.1	24,790	
Barstar*[b]	B	10,279	0.7451	2.097×10^4	4.88	10,281		9820	9900
Barstar*-Y29A	B	10,112	0.7450	1.948×10^4	4.88	10,114		9450	9700
Binase1	B	24,434	0.7271	5.386×10^4	8.82	24,429		23,390	23,250
Binase2	B	24,434	0.7271	5.386×10^4	8.82	24,423		23,390	23,400

TOF, time-of-flight. [a]Predicted mass for des-Met protein or His-tag-cleaved proteins. [b]Batch B barstar* protein was produced with a native N terminus including N-terminal Met residue (N-terminal sequence MKKAVI).

Similar experiments were performed using different concentrations of His-tagged and -untagged barstar*-Y29A, binase1 and binase2, and at different temperatures and protein concentrations, and the data are summarized in Table 2. For experiments performed using relatively high binase protein concentrations in the ITC cell (greater than ~7 μM), the binding signals for barstar*-Y29A binding to each binase site were suitable to fit the data to the two sets of sites model, as described above. However, for experiments performed using lower binase concentrations (less than ~7 μM), the binding signals for the lower-affinity site were too small to obtain a confident fit, and thus, the data for the higher-affinity site were fit independently, using a one set of sites model.

Collective analysis of the ITC data for barstar*-Y29A proteins binding to binase1 and binase2 shows that the N value for each interaction is close to 1 (N_1 = 1.03 ± 0.10, and N_2 = 0.95 ± 0.17), consistent with the proteins being of high purity, and having full fractional binding activity. For experiments performed at 25°C, the K_d values determined by the different laboratories for the high-affinity site were within a range of 8–80 nM and for the

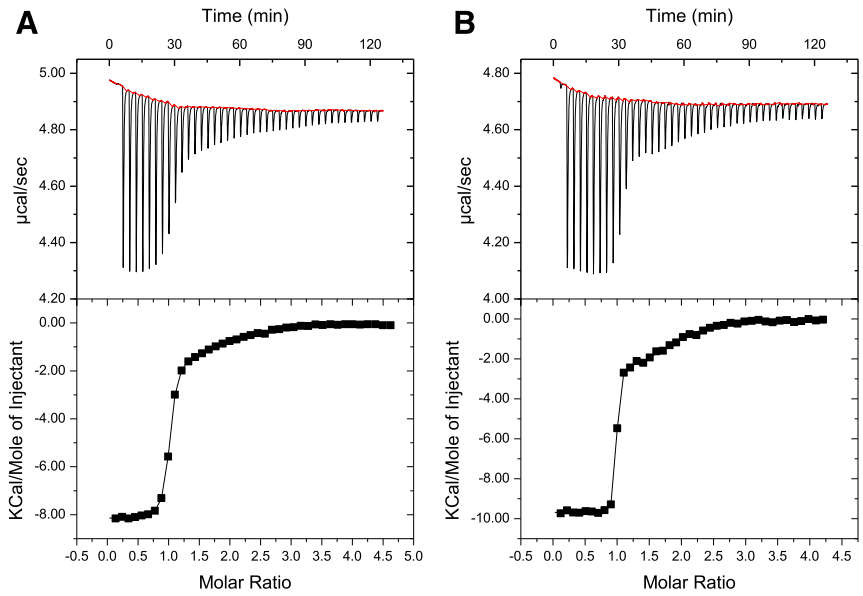

FIGURE 2

ITC data for the binding of (*A*) His-barstar*-Y29A or (*B*) His-barstar* to His-binase2 in solution. *A*) Raw calorimetric titration data (top) and integrated data (bottom) for titration of 300 μM His-barstar*-Y29A into 14 μM His-binase2 at 25°C. *B*) Raw calorimetric titration data (top) and integrated data (bottom) for titration of 273 μM His-barstar* into 14 μM His-binase2 at 25°C. Both data sets were fitted to a two sets of sites binding model.

TABLE 2

Thermodynamics of Barstar-Binase Interactions as Measured by ITC

Laboratory	Syringe	Cell	Temperature (°C)	Concentration ratio	N1	K_d1 (nM)	dH1 (kJ/M)	N2	K_d2 (μM)	dH2 (kJ/M)
D	Barstar-Y29A	Binase1	20[a]	711:27.5	0.973 ± 0.004	39 ± 6	−30.8 ± 0.1	0.79 ± 0.09	23 ± 2	−25.9 ± 3.8
D	Barstar-Y29A	Binase1	25[a]	711:27.5	0.970 ± 0.003	34 ± 2	−37.8 ± 0.1	0.94 ± 0.04	17 ± 1	−26.4 ± 1.7
C	Barstar-Y29A	Binase1	25	530:32.3	1.13 ± 0.01	15 ± 3	−28.3 ± 0.1	0.93 ± 0.04	5.0 ± 0.9	−10.7 ± 0.7
D	Barstar-Y29A	Binase1	25[a,b]	85:3.5	1.12 ± 0.01	43 ± 6	−29.5 ± 0.3			
C	Barstar-Y29A	Binase1	25[b]	259:6.41	1.12 ± 0.01	83 ± 15	−29.1 ± 0.4			
C	Barstar-Y29A	Binase1	30	527:32.6	1.10 ± 0.01	25 ± 4	−34.2 ± 0.9	1.03 ± 0.07	19 ± 3	−22.8 ± 2.4
C	Barstar-Y29A	Binase1	30[b]	259:6.41	1.16 ± 0.04	43 ± 13	−43.8 ± 2.4			
D	Barstar-Y29A	Binase1	36[a,b]	85:3.50	1.09 ± 0.01	77 ± 6	−48.1 ± 0.4			
A	His-barstar-Y29A	His-binase2	25	300:14	0.967 ± 0.002	8.1 ± 0.9	−34.2 ± 0.1	1.01 ± 0.035	2.9 ± 0.3	−7.9 ± 0.4
A	His-barstar-Y29A	His-Binase2	25	600:35	0.884 ± 0.002	19 ± 2	−43.4 ± 0.1	0.944 ± 0.021	8.7 ± 0.6	−19.8 ± 0.7
D	Barstar-Y29A	Binase2	20[a]	711:27.5	0.802 ± 0.002	32 ± 3	−32.7 ± 0.1	0.71 ± 0.07	20 ± 2	−22.2 ± 2.5
D	Barstar-Y29A	Binase2	25[a]	711:34.4	0.836 ± 0.001	19 ± 1	−38.7 ± 0.1	0.82 ± 0.01	13.9 ± 0.4	−20.9 ± 0.4
C	Barstar-Y29A	Binase2	25	530:30.3	1.07 ± 0.01	11 ± 2	−29.9 ± 0.1	1.07 ± 0.01	4.5 ± 0.8	−9.7 ± 0.5
D	Barstar-Y29A	Binase2	25[a,b]	85:4.0	1.00 ± 0.01	29 ± 3	−32.3 ± 0.2			
C	Barstar-Y29A	Binase2	25[b]	259:5.86	1.08 ± 0.01	62 ± 17	−30.4 ± 0.6			
C	Barstar-Y29A	Binase2	30	527:30.3	1.11 ± 0.01	23 ± 5	−37.1 ± 0.1	1.30 ± 0.08	12 ± 3	−15.2 ± 1.7
C	Barstar-Y29A	Binase2	30[b]	259:5.86	1.05 ± 0.01	70 ± 12	−35.7 ± 0.5			
D	Barstar-Y29A	Binase2	36[a,b]	85:4.0	1.00 ± 0.01	63 ± 8	−39.4 ± 0.4			
A	His-barstar	His-Binase1	25	273:14	0.912 ± 0.004	<2	−38.8 ± 0.1	1.00 ± 0.025	1.3 ± 0.2	−11.9 ± 0.5
A	His-barstar	His-binase1	25	273:14	0.938 ± 0.001	<2	−38.9 ± 0.1	0.913 ± 0.017	2.3 ± 0.2	−15.0 ± 0.4
A	His-barstar	His-binase2	25	273:14	0.942 ± 0.002	<2	−40.5 ± 0.1	0.931 ± 0.024	1.8 ± 0.2	−11.9 ± 0.4
A	His-barstar	His-binase2	25	600:35	0.946 ± 0.002	<2	−41.1 ± 0.1	0.895 ± 0.015	1.9 ± 0.2	−12.6 ± 0.3
A	His-barstar	His-binase2	25	35:2	0.964 ± 0.003	<2	−39.9 ± 0.2	0.964 ± 0.000	1.2 ± 0.6	−7.7 ± 1.3
A	Barstar	Binase2	25	273:14	0.956 ± 0.002	<2	−40.9 ± 0.1	0.896 ± 0.024	1.8 ± 0.2	−12.4 ± 0.5

[a]All errors were determined by nonlinear least-squares analysis. [b]Data obtained at lower concentrations of protein in the calorimeter cell were best described by a one set of sites binding model.

low-affinity site were all 3–17 μM. At higher temperatures, the interactions were more exothermic, and the binding affinity was generally weaker, as expected based on free-energy relationships.[24] Comparison of the data obtained using His-tagged *versus* -untagged proteins suggests that the presence of the His tag has little influence on the binding interactions in solution. In addition, the thermodynamic data acquired using binase1 were comparable to that for binase2, indicating that the orientation of the low- and high-affinity mutant barnase domains has an undetectable impact on barstar binding (Table 2).

For comparison to the lower-affinity Y29A mutant, laboratory A also tested the binding of the higher-affinity His-barstar* and untagged barstar* proteins to binase1 and binase2. Like the Y29A mutant, the binding curves for barstar* consisted of 1 high-affinity and 1 low-affinity interaction (Fig. 2*B*), with N values close to 1 for each site (N_1 = 0.94 ± 0.02, and N_2 = 0.93 ± 0.04), suggesting that the proteins were of high purity and full fractional activity (Table 2). However, for the wild-type barstar* protein, the binding data for the high-affinity site showed insufficient curvature to accurately determine the binding affinity, indicating that the K_d value for this interaction is too tight and several orders of magnitude lower than the concentration of binase proteins tested in the ITC cell. This was the case even for titrations performed using as low as 2 μM His-binase2 in the cell. Therefore, the lower limit of the K_d for wild-type barstar* binding to the high-affinity site of binase1 or binase2 is estimated to be <2 nM. On the other hand, the binding data for the lower-affinity binase site were well defined and showed excellent reproducibility with K_d values of 1.2–2.3 μM, for His-tagged and -untagged binase1 and binase2 (Table 2).

AUC Characterization of Barstar*-Binase Interactions

The individual barstar and binase molecules were first examined by sedimentation equilibrium as an orthogonal analysis to the SEC-MALS and DLS data to assess the protein homogeneity and to confirm that the proteins were monodisperse under concentration ranges used to measure interaction using the ultracentrifuge. The MWs for the binase constructs as determined in 2 laboratories were in excellent agreement with the expected MWs for both the His-tagged and native constructs (Table 1). The barstar* and barstar*-Y29A proteins also exhibited single, homogeneous species, with the MWs determined in laboratory E within 5% of the predicted and mass spectrometry-determined molecular masses. Repeated determinations of barstar* and barstar*-Y29A MWs in laboratory B indicated that they were ~15% higher than the predicted and mass spectrometry-measured masses, yet the samples were monodisperse. Because the values were consistently and reproducibly obtained over a year during the course of the study, they were used as parameter values in determining equilibrium constants for the barnase-barstar interactions.

Example sedimentation equilibrium data for the barstar*-Y29A complexes with binase1 or binase2 are shown in **Fig. 3*A***, *C*, and the apparent K_d values for the interactions are summarized in **Table 3**. Under the conditions tested, only laboratory E was able to confidently determine K_d values for the binding of barstar*-Y29A to the high-affinity binase site (H102A domain), obtaining K_d values for each binase protein in the 5–40 nM range, in good agreement with the ITC data. For the weaker interaction of barstar*-Y29A binding to the lower-affinity site (R59A,H102Q domain), both laboratories B and E measured K_d values between 16 and 47 μM for binding to binase1, and B measured a K_d of 60 μM (95% confidence interval of 47–76 μM) for binding to binase2. On average, these AUC-determined K_d values suggest ~5-fold lower affinity than that measured by ITC.

The complexes of His-barstar* with His-binase1 or His-binase2 were studied only in laboratory B (Fig. 3*B*, *D*). These studies yielded a K_d of 2.55 μM (2.35–2.78 μM) for binding to His-binase1 and a K_d of 3.71 μM (3.40–4.03 μM) for binding to His-binase2, which is in excellent agreement with the affinity measured by ITC (1.2–2.3 μM). The K_d for barstar* binding to the high-affinity site could not be determined because it was beyond the high-affinity range that could be accurately measured.

SPR Characterization of Barstar* Binding to Immobilized Binase Proteins

The binding interactions between barstar and binase proteins were also tested by SPR using Biacore instrumentation. In contrast to ITC and AUC, which are solution-based technologies, SPR requires immobilization or affinity capture of one of the binding partners on the sensor chip surface (referred to as the "Ligand"), with the other binding partner present free in solution (referred to as the "Analyte"). To avoid avidity effects with bivalent binase analytes in solution,[2] experiments were designed with monovalent barstar analytes in solution binding to immobilized binase ligands on the SPR sensor chip.

Figure 4*A*–*C* shows example binding data for a broad concentration series (0.57 nM–300 μM) of His-barstar*-Y29A injected over different surface densities of immobilized His-binase2. The sensorgram data show very fast association and dissociation kinetics for the His-barstar*-Y29A analyte, with equilibrium (steady-state) binding achieved during the 60-s association phase. These data were fit to a 2-site steady-state binding model, with the

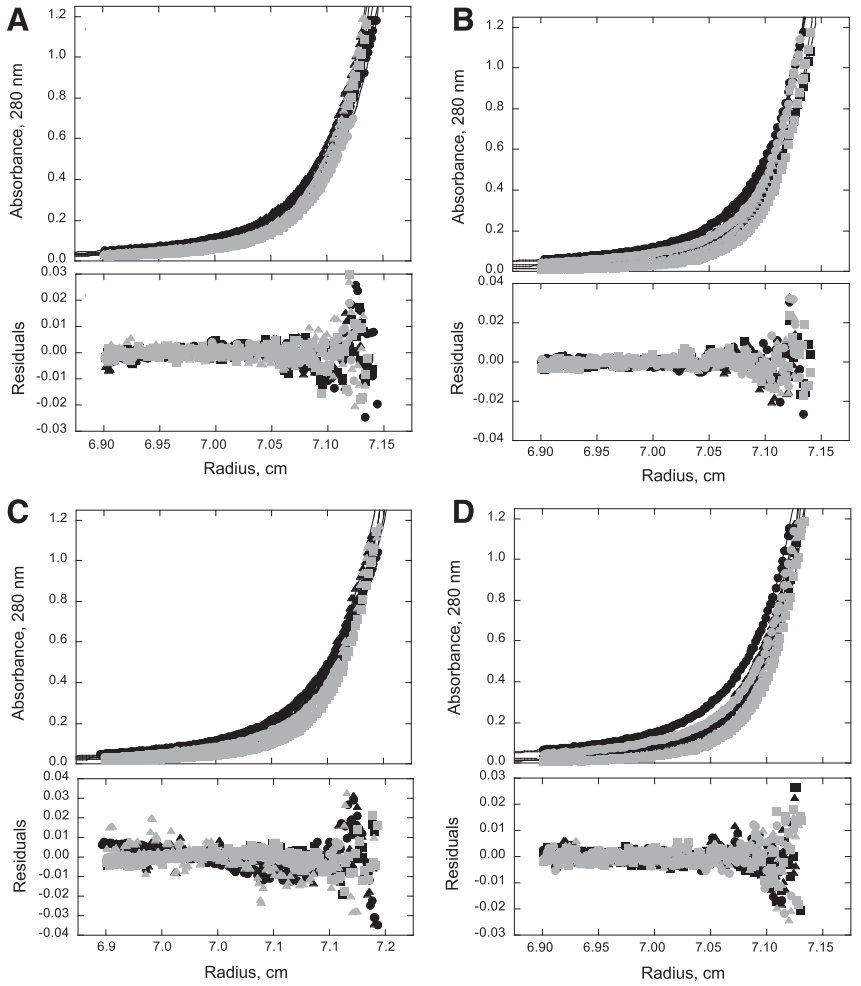

FIGURE 3

Sedimentation equilibrium data for the interaction of His-barstar* proteins with His-binase proteins. The top of each panel shows representative traces of data from 2-channel centerpieces plotted as absorbance at 280 nm *vs.* relative radial distance for different protein concentrations and at 2 different speeds (26,000 and 30,000 rpm), whereas the bottom of each panel shows residual error ($A_{theoretical} - A_{observed}$) for global analysis of the data. Each panel shows the data for a different set of binase/barstar pairs as follows: (*A*) His-binase1: His-barstar*-Y29A, (*B*) His-bainse1:His-barstar*, (*C*) His-binase2:His-barstar*-Y29A, and (*D*) His-binase2: His-barstar*. Within each panel, the symbols represent binase:barstar concentration ratios of 2.5:5.0 μM (■), 2.5:7.5 μM (▲), and 2.5:10.0 μM (●). Black and gray data points are from experiments performed at 26,000 and 30,000 rpm, respectively.

high-affinity binding of His-barstar*-Y29A to the H102Q domain of His-binase2 predominating at lower analyte concentrations and binding to the low-affinity R59A, H102Q domain occurring at high analyte concentrations (Fig. 4*D*). Triplicate measurements for His-barstar*-Y29A binding to immobilized His-binase2 show excellent reproducibility (Fig. 4*C*), with a global analysis of these 3 data sets yielding K_d values of 280 ± 18 nM for the high-affinity site and 55 ± 4 μM for the low-affinity site (**Table 4**). K_d values obtained across the different laboratories and using different combinations of His-tagged or -untagged proteins, as well as with binase1 or binase2, were generally within 2-fold of this triplicate experiment, suggesting that neither the presence of the His tag nor the orientation of the 2 barnase domains has a significant influence on barstar* binding (Table 4). Collective analysis of the SPR data from all laboratories including His-tagged, -untagged, binase1, and binase2

TABLE 3

K_d Values for Barstar-Binase Interactions from AUC Equilibrium Sedimentation Data at 25°C

		Barstar*-Y29A		Barstar*	
Laboratory[a]	Protein	K_d1 (nM)	K_d2 (range)	K_d1 (nM)	K_d2 (range)
E	Binase1	10–40	46 μM (35–57)		
E	Binase1	5–15	18 μM (14–22)		
E	Binase2	10–40			
B	His-binase1		47 μM (40–56)		2.6 μM (2.4–2.8)
B	His-binase2		60 μM (47–76)		3.7 μM (3.4–4.0)

[a]Data from laboratory B were acquired using His-tagged barstar and binase proteins, whereas data from laboratory E were acquired using untagged barstar and binase proteins.

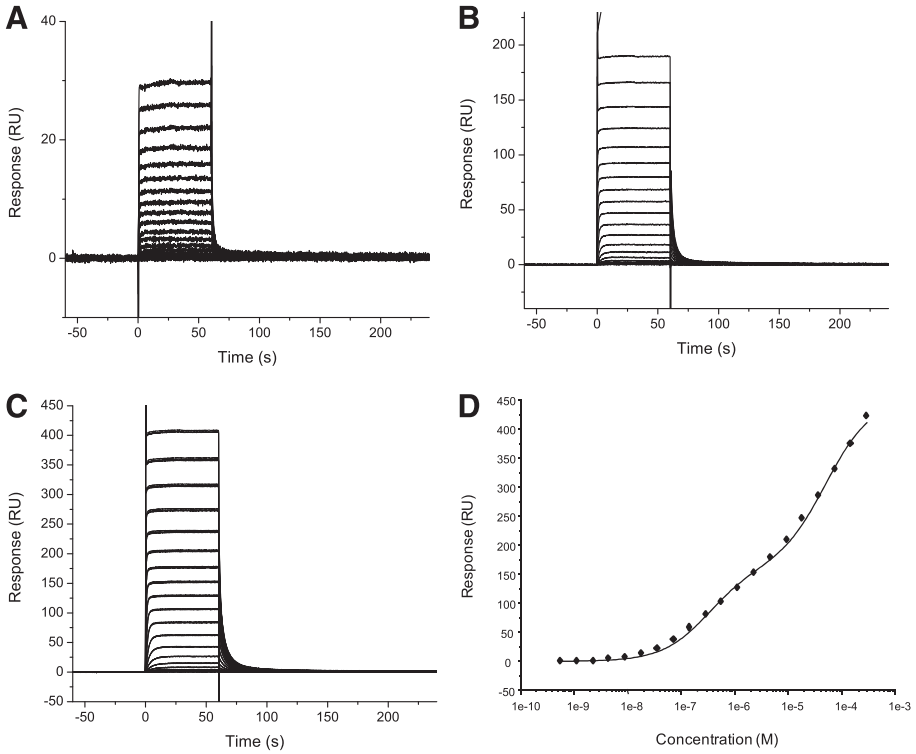

FIGURE 4

SPR data for the binding of barstar*-Y29A to immobilized His-binase2. Sensorgram data for 300 μM–0.56 nM (2-fold dilutions) His-barstar*-Y29A binding to (*A*) 107 RU His-binase2, (*B*) 518 RU His-binase2, or (*C*) 1011 RU His-binase2. The data in (*C*) represent 3 experiments. *D*) Example equilibrium response data obtained in triplicate on the 1011 RU His-binase2 surface and fit to a 2-site steady-state binding model to determine the equilibrium binding constant for His-barstar*-Y29A binding to each domain of His-binase2.

proteins yields an average K_d value with SD for the high-affinity site of 340 ± 140 nM and for the low-affinity site of 78 ± 48 μM, showing good reproducibility in K_d determination using SPR across different laboratories. Interestingly, however, the SPR-determined binding affinities were significantly weaker than those determined by ITC and AUC, especially for the high-affinity site that differed by an order of magnitude.

Similar SPR experiments were performed in laboratory A to evaluate the binding of barstar* to immobilized binase proteins. The SPR sensorgram data appear qualitatively similar to that for the Y29A mutant, except that the dissociation of His-barstar* is much slower than for His-barstar*-Y29A, particularly at lower analyte concentrations where the high-affinity binding interaction dominates (**Fig. 5** ***A***–*C*). Because equilibrium is not achieved at these lower concentrations, a 2-site steady-state binding model could not be employed to fit the data. Attempts to fit the data to a 2-site kinetic model were also unsuccessful due to the rapid kinetics, particularly at the lower-affinity site. Consequently, the best representation of the data and highest reproducibility were obtained by separately fitting the lower-concentration analyte data to a 1:1 Langmuir kinetic model and the higher-concentration analyte data to a 1:1 steady-state model (Fig. 5*D*). The estimated binding affinities from this analysis were similar for His-tagged and -untagged barstar* proteins binding to His-tagged or -untagged binase1 or binase2, with K_d values of ~6–13 nM for the higher-affinity interaction and K_d values of ~39–54 μM for the lower-affinity interaction (Table 4). Collective analysis of all barstar* data provides an estimate for the K_d value for the higher-affinity site to be 8.8 ± 2.0 nM and 40 ± 11 μM for the lower-affinity site, which are ~1 order of magnitude lower affinity than the K_d values determined by ITC and AUC.

SPR Characterization of Barstar* Binding to Anti-His-Captured Binase Proteins

Taking advantage of the N-terminal His tag on the His-binase molecules, we also performed studies using a His-tag capture SPR format. His-tag capture has the advantage of orientating the His-binase proteins on the surface and also eliminating the potential heterogeneity that would result from random amine coupling to the 16 different Lys residues or N terminus of the protein. For these experiments, His-binase2 was captured at 3 different surface densities on an immobilized anti-His Fab surface, and the binding of untagged barstar*-Y29A or barstar* was tested under identical analyte concentrations and solution conditions as the immobilized binase experiments described above.

Figure 6*A*, *D* shows SPR sensorgram data for the capture of His-binase2 and binding of 0.57 nM–300 μM barstar*-Y29A or barstar*, respectively. Because

TABLE 4

K_d Values for Barstar-Binase Interactions from SPR Data at 25°C Using Amine-Coupled Binase Proteins

			His-barstar-Y29A		Barstar-Y29A		His-barstar		Barstar	
Lab	Ligand	Density (RU)	K_d1 (nM)	K_d2 (μM)	K_d1 (nM)	K_d2 (μM)	K_d1 (nM)	K_d2 (μM)	K_d1 (nM)	K_d2 (μM)
A	His-binase1	997.3	320 ± 39	52 ± 6			13	41 ± 9	12	25 ± 4
		997.3	320 ± 37	51 ± 6			12	39 ± 9		
		997.3	370 ± 46	53 ± 7			10	40 ± 10		
		Global	340 ± 21	52 ± 3			12	40 ± 4		
F	Binase1	300			440 ± 8	90 ± 2				
F	Binase1	1000			530 ± 8	89 ± 2				
F	Binase1	3000			660 ± 10	98 ± 2				
G	Binase1	1000			290 ± 5	38 ± 1				
A	His-binase2	107	470 ± 56	74 ± 9	360 ± 31	63 ± 6	6.7	46 ± 5		
A	His-binase2	518	300 ± 36	64 ± 9	260 ± 23	61 ± 7	8.8	54 ± 10		
A	His-binase2	1010.7	260 ± 32	54 ± 7			8.6	49 ± 10	8.5	34 ± 5
		1010.7	260 ± 31	53 ± 7			8	48 ± 11		
		1010.7	330 ± 42	58 ± 8			7.1	48 ± 11		
		Global	280 ± 18	55 ± 4			7.9	48 ± 5		
A	Binase2	995.5	250 ± 33	58 ± 8			7.7	54 ± 11	7.4	35 ± 5
		995.5	250 ± 33	57 ± 7			7.1	53 ± 12		
		995.5	330 ± 45	62 ± 9			6.4	52 ± 12		
		Global	270 ± 19	59 ± 4			7.1	53 ± 6		
F	Binase2	40			320 ± 10	240 ± 10				
F	Binase2	300			330 ± 7	86 ± 3				
F	Binase2	1100			400 ± 10	134 ± 5				
F	Binase2	2500			420 ± 20	87 ± 9				
G	Binase2	1000			95 ± 8	40 ± 5				

All errors were determined by nonlinear least-squares analysis.

the His-tag dissociation rate is on the order of 10^{-3} s^{-1}, a consistent dissociation of the protein from the surface is observed during each analyte binding-dissociation cycle. However, because the dissociation is highly reproducible between cycles, this baseline drift can be partially accounted for using "double referencing," which involves subtracting data from the reference surface as well as control injections of running buffer.[25]

Example double-referenced sensorgram data are shown in Fig. 6*B*, *E*. Overall, the sensorgram data show similar kinetic profiles to the experiments conducted on immobilized binase surfaces. In particular, barstar*-Y29A rapidly achieves equilibrium binding at all concentrations tested and dissociates rapidly (Fig. 6*B*), whereas the high-affinity site of wild-type barstar* demonstrates much slower dissociation properties and does not reach equilibrium at lower analyte concentrations (Fig. 6*E*). Careful inspection of the sensorgram data also shows a small, consistent, and reproducible decrease in response during the analyte injection after an apparent "steady state" is achieved. This is most likely because the binding of barstar* slows the recapture rate of His-binase2 on the anti-His surface; in other words, the association rate for the His-binase2/barstar* complex on the anti-His surface is slower than that for His-binase2 alone. Although this results in slightly different "steady-state" responses at different time points in the association data, the fitted K_d values were similar regardless of which region of the sensorgram data was analyzed. The resulting data also fit well to the 2-site steady-state model for barstar*-Y29A (Fig. 6*C*) or the separate Langmuir and steady-state models for wild-type barstar* (Fig. 6*F*) that were used in the immobilized binase experiments, further supporting that these binding models were reasonable representations of the data. The resulting K_d values for barstar*-Y29A (~50 nM and ~30 μM) and barstar* (~5 nM and 10–15 μM) were significantly lower than those obtained in the immobilized binase format and either within or close to the range of K_d values obtained by ITC and AUC (**Table 5**).

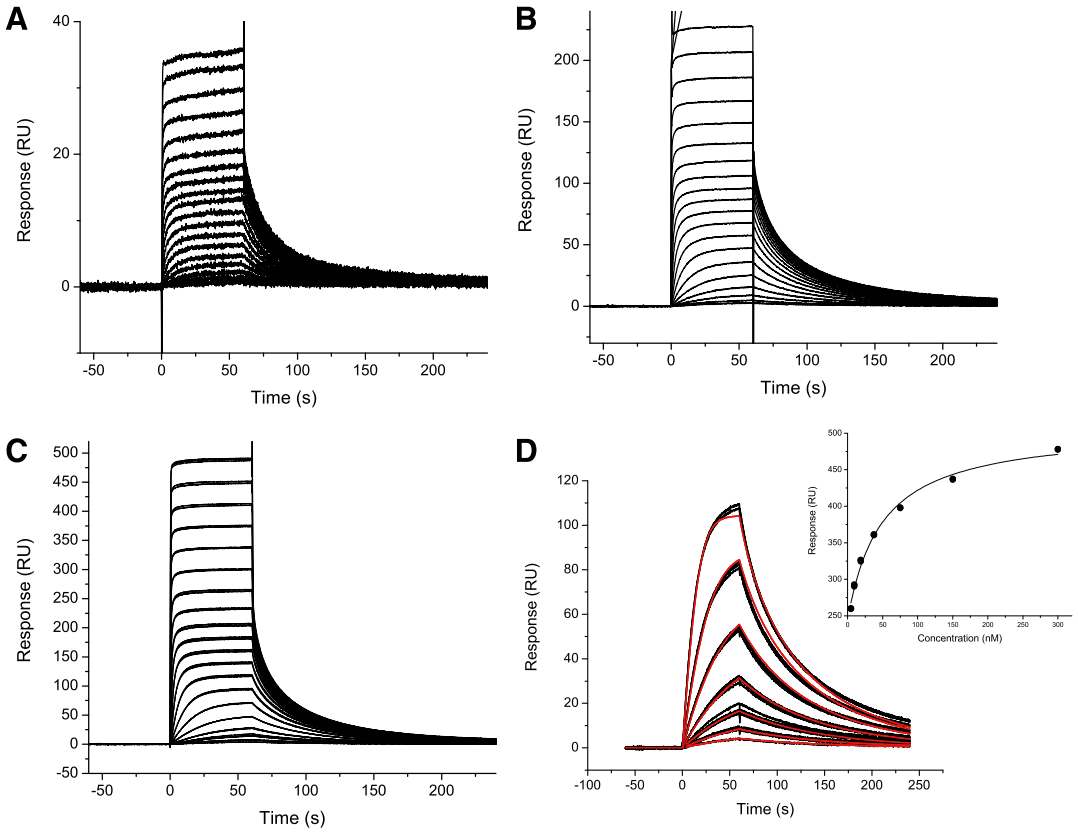

FIGURE 5

SPR data for the binding of barstar* to immobilized His-binase2. Sensorgram data for 300 μM–0.56 nM (2-fold dilutions) His-barstar* binding to (*A*) 107 RU His-binase2, (*B*) 518 RU His-binase2, or (*C*) 1011 RU His-binase2. The data in (*C*) represent 3 experiments. *D*) Example fitted triplicate data on the 1011 RU His-binase2 surface, where the lower analyte concentration data (37–0.57 nM) are fit to a 1:1 Langmuir kinetic model, and the higher analyte concentration data (300–4.7 μM) are fit to a 1:1 steady-state binding model to estimate the kinetic and affinity values for His-barstar* binding to each domain of His-binase2.

DISCUSSION

The objective of the current MIRG study was to develop a challenging protein-protein interaction system that could be used to evaluate the capabilities of different users and different biomolecular interaction technologies to accurately determine K_d values for a 2-site macromolecular system in the nanomolar-to-micromolar affinity range. This affinity range was of interest because it is the most commonly studied range for biologic interactions, in particular, those studied in the core laboratories of the ABRF. The subject of the study was the interaction of barstar*-Y29A with binase. The system was characterized and evaluated by ITC, AUC, and SPR in multiple MIRG laboratories. The proteins for use in the interaction analysis were prepared as His-tagged and native polypeptides, and in addition, the binase constructs were prepared with different orientations of the high- and low-barnase domains. Analysis of the data obtained from each technique indicates that neither the presence nor absence of the His tag nor the orientation of the binase domains has a significant influence on the binding interactions. This is consistent with the structure of the barstar-barnase complex, in which the N-terminal region of barnase lies on the opposite surface of the protein from the barstar binding interface[26] (**Fig. 7**). Because the different constructs compare so favorably, the binding data for barstar*-Y29A were collectively summarized in **Fig. 8** without distinction between His-tagged *versus* -untagged or binase1 *versus* binase2 constructs.

Comparison of the data in Tables 2, 3, 4, and 5 shows excellent reproducibility in characterizing a given interaction in a given laboratory and good reproducibility across different laboratories. However, differences in the K_d determinations using ITC and SPR are noted (Fig. 8). The average K_d values for barstar*-Y29A binding to the binase proteins as determined from all the 25°C ITC data were 32 ± 24 nM for the higher-affinity site and

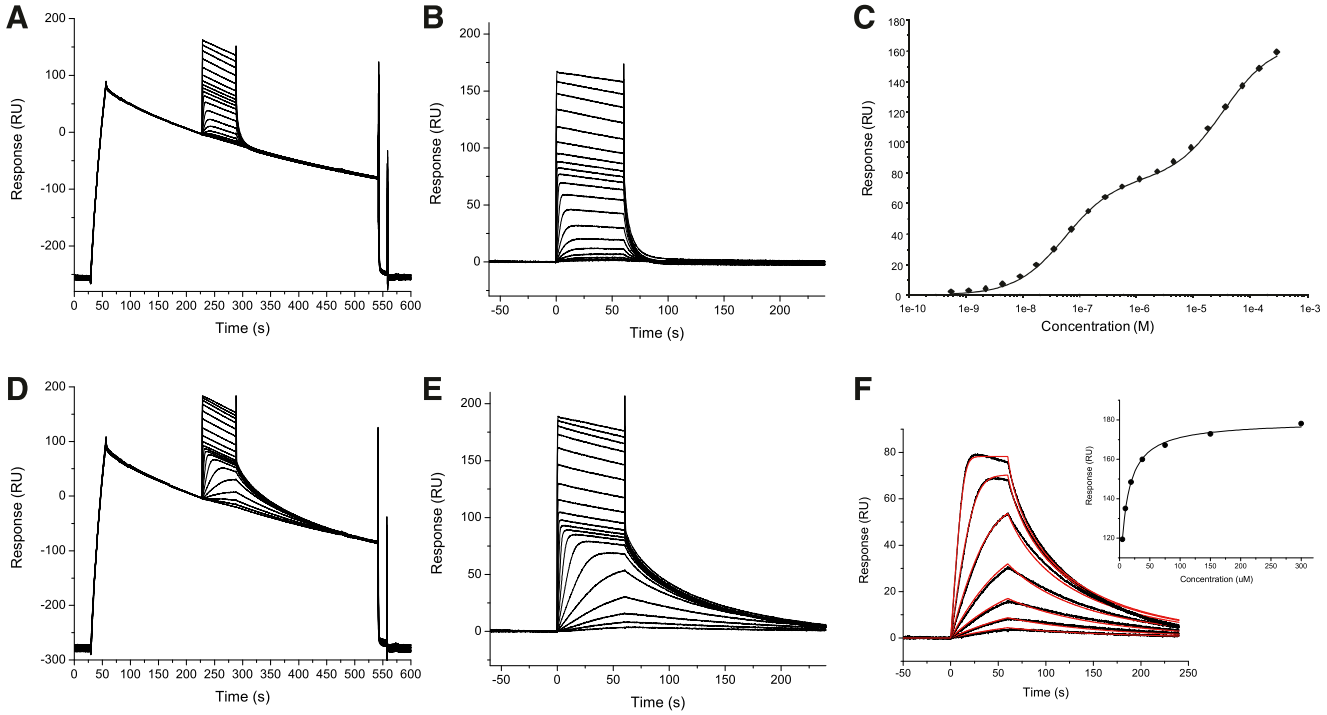

FIGURE 6

SPR data for the binding of barstar*-Y29A or barstar* to anti-His-captured His-binase2. Sensorgram data for the capture of 5 μg/ml His-binase2 followed by 300 μM–0.56 nM (2-fold dilutions) of (*A*) untagged barstar*-Y29A or (*D*) untagged barstar*. Double-referenced sensorgram data for (*B*) untagged barstar*-Y29A or (*E*) untagged barstar*. *C*) Equilibrium response data for barstar*-Y29A fit to a 2-site steady-state binding model to determine the equilibrium binding constant for untagged barstar*-Y29A binding to each domain of His-binase2. *F*) Kinetic data for 37–0.57 nM untagged barstar* fit to a 1:1 Langmuir kinetic model, or 300–4.7 μM fit to a 1:1 steady-state binding model, to estimate the kinetic and affinity values for barstar* binding to each domain of His-binase2.

8.7 ± 5.7 μM for the lower-affinity site. The binding affinities for wild-type barstar* were only measured in 1 laboratory and were found to be <2 nM and ~2 μM for the 2 binase domains. This corresponds to approximately a 2-order of magnitude difference in affinity at the 2 binding sites of the binase molecules, in agreement with data reported by other groups for the monovalent mutant proteins.[4,7,8,27] The barstar*-Y29A K_d values determined by SPR on immobilized binase surfaces for the higher-affinity site (340 ± 140 nM) and lower-affinity site (78 ± 48 μM) were ~10-fold weaker than those determined by ITC (Fig. 8). However, the K_d values determined using anti-His-captured His-binase (K_d1, ~50 nM, and K_d2, ~30 μM) were much closer to those determined by ITC and were even in the range of the ITC data for the higher-affinity site. Similar trends were also observed for wild-type barstar*, with ~10-fold lower SPR affinity toward immobilized binase surfaces as compared with ITC and intermediate affinity for anti-His-captured binase surfaces. Although the current data set obtained by AUC is considerably smaller than that obtained by ITC or SPR, the AUC-determined affinity of barstar*-Y29A for the

TABLE 5

K_d Values for Barstar-Binase Interactions from SPR Data at 25°C Using Anti-His-Captured Binase Proteins

			Barstar-Y29A		Barstar	
Laboratory	Proteins	Density (RU)	K_d1 (nM)	K_d2 (μM)	K_d1 (nM)	K_d2 (μM)
A	His-binase2	315	56 ± 2	34 ± 2	4.7	11 ± 2
A	His-binase2	450	48 ± 2	29 ± 2	4.1	15 ± 4
A	His-binase2	640	53 ± 2	31 ± 2	5.4	10 ± 1

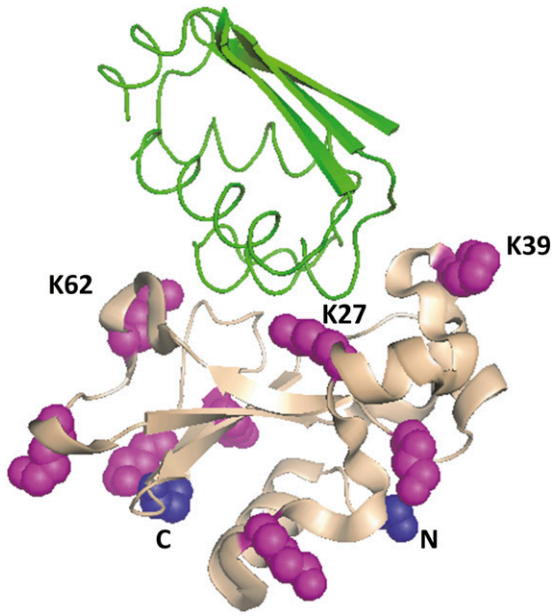

FIGURE 7

Structure of the barstar-barnase complex (Protein Data Bank 1BRS). Barstar is shown in green ribbon representation, whereas barnase is shown in light gray. The Lys side chains in barstar are shown in magenta space-fill representation, whereas the N and C termini are shown in blue space fill and labeled "N" and "C," respectively.

high-affinity site (K_d, 5–40 nM) was in good agreement with the ITC data, whereas that for the lower-affinity site (K_d, ~46–47 μM) was more comparable to the SPR data. For wild-type barstar*, only the K_d for the lower-affinity site was obtained by AUC (~3 μM), which also agreed better with the ITC and anti-His capture SPR measurements.

Given the wealth of literature showing good agreement between affinities determined by SPR and ITC, for example [1,28–30], the lower SPR-determined affinity for barstar*-Y29A binding to binase proteins was somewhat unexpected. In the relatively few reported cases in which affinity measurements disagree between these technologies, the differences have generally been attributed to incorrect assumptions on the valency, oligomeric state, or the model used to fit the data.[31,32] In the present study, however, the barnase-barstar interaction is extremely well characterized. Additionally, the protein molecules used in the present study were highly pure and monomeric (Table 1) and had the expected integral numbers of binding sites (Table 2). Thus, it seems likely that there are intrinsic differences between the solution-based surface-based measurements for the binase-barstar system.

One possibility is that surface heterogeneity could influence the binding activity. For example, each of the 2 barnase domains contains 8 Lys residues in addition to the N terminus, for a total of 17 potential immobilization sites on each binase protein. Of these sites, only immobilization at Lys27 would be expected to completely preclude barstar binding because this residue is located at the center of the binding site and is critically important for the high-affinity interaction.[7,26,33] Indeed, immobilization at this site may at least partially account for the ~30% lower overall surface activity of the immobilized binase surfaces compared to anti-His-captured binase surfaces. However, other Lys residues such as Lys39 and Lys62, although not directly involved in barstar binding, are adjacent to the binding interface and have been shown to have reduced solvent accessibility in complex with barstar.[34] Thus, it is plausible that immobilization at these, and possibly other, sites could influence binding kinetics and reduce affinity without completely preventing barstar binding. The use of anti-His-captured surfaces would be expected to alleviate this issue, which is consistent with the increased binding affinity measured in this SPR format compared to experiments using amine coupling.

Another parameter that could result in the lower affinities seen in SPR measurements is the electrostatic effects on the SPR sensor chip surface. The binase proteins

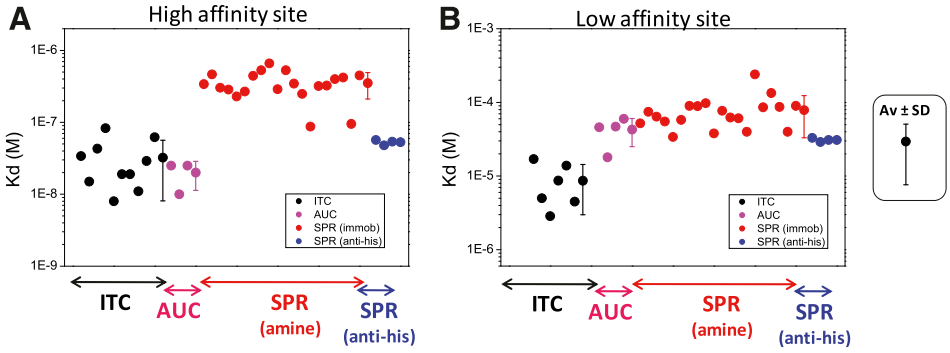

FIGURE 8

Summary of K_d values for barstar*-Y29A binding to binase proteins. All data obtained at 25°C for His-tagged and -untagged proteins as well as binase1 and binase2 are represented without distinction. *A*) Data for binding to the higher-affinity site (H102Q domain). *B*) Data for binding to the lower-affinity site (R59A,H102Q domain). Data obtained using different techniques are represented by different colors. The rightmost data point (with error bars) for each technique represents the average and SD of the K_d values for that technique. Note that triplicate SPR data are represented by a single point from the global analysis of 3 experiments. The error for this triplicate SPR measurement is contained within the size of the symbol.

are highly basic (theoretical pI, ~8.5–8.8), whereas the barstar proteins are very acidic (theoretical pI, ~4.9–5.3) (Table 1). For the interaction in solution, these opposite charges drive strong electrostatic steering effects that facilitate the unusually fast association and high affinity of binding for barnase-barstar compared with other protein-protein interactions.[3] In a surface-based SPR experiment, however, the flexible and acidic dextran chip matrix may interact with immobilized binase and/or repel the acidic barstar analyte to reduce the apparent binding affinity. These electrostatic effects may explain why the K_d values determined in the anti-His-captured format, although lower than those determined in the immobilized SPR format, are still higher than the K_d values determined by ITC. Similar effects have also been shown for other protein pairs of similar charge using the standard Biacore CM5 sensor chips.[35] The reduced anti-His recapture rate implied by the sensorgram data in Fig. 6 and described in the RESULTS' section for the His-binase2-barstar*-Y29A complexes is also consistent with these types of electrostatic effects. Future experiments could test this hypothesis, for example, using Biacore chips with lower acidic charge including Biacore CM4 or C1 chips (GE Healthcare Bio-Sciences).

Compared to the previous MIRG study of the simpler 1:1 binding of CA-II to its small molecule inhibitor CBS, the present study provided additional complexities in the form of bivalency for one of the binding partners, as well as the large affinity difference at the 2 binding sites. These complexities increase the challenges of appropriately processing and fitting the more complex binding curves, as well as working within the appropriate protein concentration range to accurately detect each interaction. Although we found some unexpected differences in K_d determination between surface-based and solution-based measurements, the affinity values measured with each technique demonstrated good lab-to-lab reproducibility. These attributes indicate that the barstar*-Y29A-binase system would be a useful tool for benchmarking new technologic approaches and training users on complex systems to increase their ability to confidently and quantitatively measure biomolecular interactions.

ACKNOWLEDGMENTS

Certain commercial materials, instruments, and equipment are identified in this manuscript in order to specify the experimental procedure as completely as possible. In no case does such identification imply a recommendation or endorsement by the Association of Biomolecular Resource Facilities or the Molecular Interactions Research Group, nor does it imply that the materials, instruments, or equipment identified are necessarily the best available for the purpose.

REFERENCES

1. Myszka DG, Abdiche YN, Arisaka F, Byron O, Eisenstein E, Hensley P, Thomson JA, Lombardo CR, Schwarz F, Stafford W, Doyle ML. The ABRF-MIRG'02 study: assembly state, thermodynamic, and kinetic analysis of an enzyme/inhibitor interaction. *J Biomol Tech* 2003;14:247–269.
2. Yamniuk AP, Edavettal SC, Bergqvist S, Yadav SP, Doyle ML, Calabrese K, Parsons JF, Eisenstein E. ABRF-MIRG benchmark study: molecular interactions in a three-component system. *J Biomol Tech* 2012;23:101–114.
3. Schreiber G, Fersht AR. Rapid, electrostatically assisted association of proteins. *Nat Struct Biol* 1996;3:427–431.
4. Frisch C, Schreiber G, Johnson CM, Fersht AR. Thermodynamics of the interaction of barnase and barstar: changes in free energy versus changes in enthalpy on mutation. *J Mol Biol* 1997;267:696–706.
5. Frisch C, Fersht AR, Schreiber G. Experimental assignment of the structure of the transition state for the association of barnase and barstar. *J Mol Biol* 2001;308:69–77.
6. Yakovlev GI, Moiseyev GP, Protasevich II, Ranjbar B, Bocharov AL, Kirpichnikov MP, Gilli RM, Briand CM, Hartley RW, Makarov AA. Dissociation constants and thermal stability of complexes of Bacillus intermedius RNase and the protein inhibitor of Bacillus amyloliquefaciens RNase. *FEBS Lett* 1995;366:156–158.
7. Schreiber G, Fersht AR. Energetics of protein-protein interactions: analysis of the barnase-barstar interface by single mutations and double mutant cycles. *J Mol Biol* 1995;248:478–486.
8. Wang T, Tomic S, Gabdoulline RR, Wade RC. How optimal are the binding energetics of barnase and barstar? *Biophys J* 2004;87:1618–1630.
9. Deyev SM, Waibel R, Lebedenko EN, Schubiger AP, Plückthun A. Design of multivalent complexes using the barnase*barstar module. *Nat Biotechnol* 2003;21:1486–1492.
10. Hartley RW. Barnase-barstar interaction. *Methods Enzymol* 2001;341:599–611.
11. Schreiber G. Methods for studying the interaction of barnase with its inhibitor barstar. *Methods Mol Biol* 2001;160:213–226.
12. Hartley RW. Barnase and barstar. Expression of its cloned inhibitor permits expression of a cloned ribonuclease. *J Mol Biol* 1988;202:913–915.
13. Wiseman T, Williston S, Brandts JF, Lin LN. Rapid measurement of binding constants and heats of binding using a new titration calorimeter. *Anal Biochem* 1989;179:131–137.
14. Laue TM, Shah BD, Ridgeway TM, Pelletier SL. Computer-aided interpretation of analytical sedimentation data for proteins. In *Analytical Ultracentrifugation in Biochemistry and Polymer Science* (Harding SE, Rowe AJ, and Horton JC, eds.), p. 90–125. London: Royal Society of Chemistry, 1992.
15. Johnson ML, Correia JJ, Yphantis DA, Halvorson HR. Analysis of data from the analytical ultracentrifuge by nonlinear least-squares techniques. *Biophys J* 1981;36:575–588.
16. Roark DE. Sedimentation equilibrium techniques: multiple speed analyses and an overspeed procedure. *Biophys Chem* 1976;5:185–196.
17. Johnson ML, Fraser SG. Nonlinear least-squares analysis. *Methods Enzymol* 1985;117:301–342.
18. Philo JS. A method for directly fitting the time derivative of sedimentation velocity data and an alternative algorithm for calculating sedimentation coefficient distribution functions. *Anal Biochem* 2000;279:151–163.
19. Stafford WF III. Boundary analysis in sedimentation transport experiments: a procedure for obtaining sedimentation coefficient distributions using the time derivative of the concentration profile. *Anal Biochem* 1992;203:295–301.

20. Schuck P, Rossmanith P. Determination of the sedimentation coefficient distribution by least-squares boundary modeling. *Biopolymers* 2000;54:328–341.
21. Behlke J, Ristau O. A new approximate whole boundary solution of the Lamm differential equation for the analysis of sedimentation velocity experiments. *Biophys Chem* 2002;95: 59–68.
22. Navratilova I, Eisenstien E, Myszka DG. Measuring long association phases using Biacore. *Anal Biochem* 2005;344: 295–297.
23. Myszka DG, Morton TA. CLAMP: a biosensor kinetic data analysis program. *Trends Biochem Sci* 1998;23:149–150.
24. Doyle ML, Hensley P. Tight ligand binding affinities determined from thermodynamic linkage to temperature by titration calorimetry. *Methods Enzymol* 1998;295:88–99.
25. Myszka DG. Improving biosensor analysis. *J Mol Recognit* 1999;12:279–284.
26. Buckle AM, Schreiber G, Fersht AR. Protein-protein recognition: crystal structural analysis of a barnase-barstar complex at 2.0-A resolution. *Biochemistry* 1994;33:8878–8889.
27. Hartley RW. Directed mutagenesis and barnase-barstar recognition. *Biochemistry* 1993;32:5978–5984.
28. Day YS, Baird CL, Rich RL, Myszka DG. Direct comparison of binding equilibrium, thermodynamic, and rate constants determined by surface- and solution-based biophysical methods. *Protein Sci* 2002;11:1017–1025.
29. Jecklin MC, Schauer S, Dumelin CE, Zenobi R. Label-free determination of protein-ligand binding constants using mass spectrometry and validation using surface plasmon resonance and isothermal titration calorimetry. *J Mol Recognit* 2009;22: 319–329.
30. Bergqvist S, Croy CH, Kjaergaard M, Huxford T, Ghosh G, Komives EA. Thermodynamics reveal that helix four in the NLS of NF-kappaB p65 anchors IkappaBalpha, forming a very stable complex. *J Mol Biol* 2006;360:421–434.
31. Lo YC, Maddineni U, Chung JY, Rich RL, Myszka DG, Wu H. High-affinity interaction between IKKbeta and NEMO. *Biochemistry* 2008;47:3109–3116.
32. Ladbury JE, Lemmon MA, Zhou M, Green J, Botfield MC, Schlessinger J. Measurement of the binding of tyrosyl phosphopeptides to SH2 domains: a reappraisal. *Proc Natl Acad Sci USA* 1995;92:3199–3203.
33. Guillet V, Lapthorn A, Hartley RW, Mauguen Y. Recognition between a bacterial ribonuclease, barnase, and its natural inhibitor, barstar. *Structure* 1993;1:165–176.
34. Jones DN, Bycroft M, Lubienski MJ, Fersht AR. Identification of the barstar binding site of barnase by NMR spectroscopy and hydrogen-deuterium exchange. *FEBS Lett* 1993;331:165–172.
35. Drake AW, Tang ML, Papalia GA, Landes G, Haak-Frendscho M, Klakamp SL. Biacore surface matrix effects on the binding kinetics and affinity of an antigen/antibody complex. *Anal Biochem* 2012;429:58–69.